



# LLIC: Large Receptive Field Transform Coding with Adaptive Weights for Learned Image Compression

Wei Jiang , Peirong Ning , Jiayu Yang , Yongqi Zhai , Feng Gao , *Member, IEEE*,  
Ronggang Wang , *Member, IEEE*

**Abstract**—Effective Receptive field (ERF) plays an important role in transform coding, which determines how much redundancy can be removed at most during transform and how many spatial priors can be utilized to synthesize textures during inverse transform. Existing methods rely on stacks of small kernels, whose ERF remains not large enough instead, or heavy non-local attention mechanisms, which limit the potential of high resolution image coding. To tackle this issue, we propose Large Receptive Field Transform Coding with Adaptive Weights for Learned Image Compression (LLIC). Specifically, for the *first* time in learned image compression community, we introduce *a few* large kernel-based depth-wise convolutions to reduce more redundancy while maintaining modest complexity. Due to wide range of image diversity, we propose to enhance the adaptability of convolutions via generating weights in a self-conditioned manner. The large kernels cooperate with non-linear embedding and gate mechanisms for better expressiveness and lighter point-wise interactions. We also investigate improved training techniques to fully exploit the potential of large kernels. In addition, to enhance the interactions among channels, we propose the adaptive channel-wise bit allocation via generating channel importance factor in a self-conditioned manner. To demonstrate the effectiveness of proposed transform coding, we align the entropy model to compare with existing transform methods and obtain models LLIC-STF, LLIC-ELIC, LLIC-TCM. Extensive experiments demonstrate our proposed LLIC models have significant improvements over corresponding baselines and achieve state-of-the-art performances and better trade-off between performance and complexity.

**Index Terms**—Transform coding, Learned image compression.

## I. INTRODUCTION

Learned image compression [1]–[5] becomes an active research area in recent years. Several models [6]–[14] have surpassed the advanced non-learned image codec Versatile Video Coding (VVC) Intra [15]. Most learned image compression models are based on variational autoencoders (VAEs) [16]. In this framework, the input image is first transformed to a latent representation by an analysis transform, the latent representation is quantized for entropy coding, and a synthesis transform is employed to map the quantized latent representation to pixels. The advantages of the learned image compression over non-learned codecs are the end-to-end optimization and *non-linear* transform coding [17].

The improvements in rate-distortion performance of learned image compression in recent years can be traced back to the

Wei Jiang, Peirong Ning, Jiayu Yang, Yongqi Zhai, Ronggang Wang are with Shenzhen Graduate School, Peking University, 518055 Shenzhen, China (email: [wei.jiang1999@outlook.com](mailto:wei.jiang1999@outlook.com)).

Yongqi Zhai, Ronggang Wang are with Peng Cheng Laboratory, 518000 Shenzhen, China.

Feng Gao is with School of Arts, Peking University, 100871, Beijing, China. Ronggang Wang is the corresponding author.

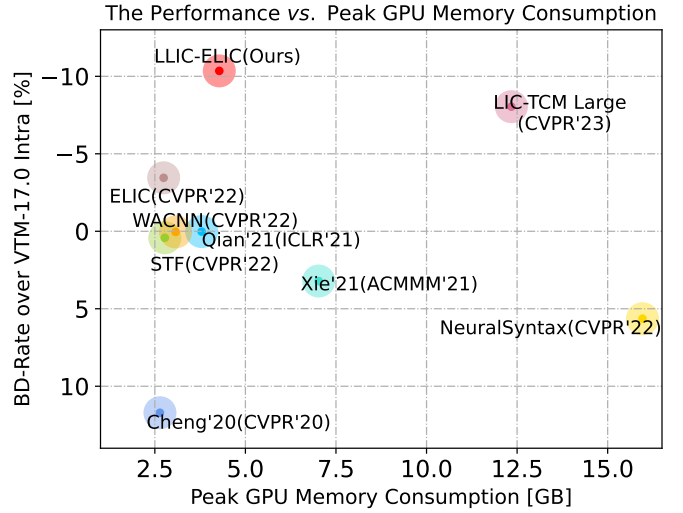


Fig. 1. BD-Rate-peak GPU Memory Consumption during testing on CLIC Pro Valid [18] with 2K resolution. Our LLIC-ELIC achieves a better trade-off between performance and GPU memory consumption.

development of nonlinear transform coding [17]. The inherent non-linearity of such coding empowers the conversion of an input image to a more compact latent representation, typically requiring fewer bits for compression. Receptive field plays an important role in transform coding, which determines how much redundancy can be removed at most and how compact the latent representation is. In addition, large receptive field helps generate more accurate textures from more spatial priors during synthesis transform. The effective receptive field is more important for high-resolution image coding, due to more spatial correlations. For example, in VVC, the largest size of coding unit is  $128 \times 128$  ( $64 \times 64$  in High Efficiency Video Coding), which ensures the long-range dependencies can be captured in high resolution images. Most earlier nonlinear transform coding techniques [1], [3]–[5], [8], [10]–[13], [19]–[22] rely on stacks of small kernels (e.g.  $3 \times 3$ ,  $5 \times 5$ ) to enlarge the receptive field. However, the effective receptive fields (ERFs) [23] of stacks of small kernels are still limited, which are illustrated in Fig. 8. To enlarge the receptive field, non-local attention [14], [24], [25] is employed, however, the inherent quadratic complexity limits the potential for high resolution image coding. Overall, enlarging the effective receptive field of nonlinear transform coding with acceptable complexity remains a challenge.

To our knowledge, large kernel design to achieve large receptive field for transform coding is overlooked. What if we use *a few large* kernels instead of *many small* kernels to

convolutional neural networks (CNNs)? In addition, due to the wide range of image diversity, the optimal transform coding for each image may be different. Compared with existing attention-based or transformer-based transform coding techniques [6], [7], [11], [14], [19], [25], the fixed convolutional weights during testing are less flexible and adaptive. Based on above considerations, we introduce a novel Spatial Transform Block (STB) with large receptive field and adaptability. Specifically, for the *first* time in learned image compression community, we propose to employ depth-wise large kernels whose size ranges from  $9 \times 9$  to  $11 \times 11$  to achieve a good trade-off between performance and efficiency. To enhance the *adaptability* of convolution weights, we propose generating the depth-wise kernel weights by using the input feature as condition with a progressive down-sampling strategy. To argument the non-linearity of transform, we propose depth-wise residual block for non-linear embedding. Moreover, gate block is proposed for low complexity point-wise interactions. In addition, we propose a simple yet effective training technique which uses large patches to fully exploit the potential of large kernels. Thanks to the proposed spatial transform with large receptive fields and adaptability, our proposed transform coding achieves much larger effective receptive fields with smaller depth, which are illustrated in Fig. 8 and the complexity is still modest.

Large adaptive depth-wise kernels are effective to reduce spatial redundancy, however, the adaptive interactions among channels are limited. Considering that different channels in a latent representation carry distinct information, it is more efficient to allocate more bits on important channels. To address this issue and inspired by Channel Attention [26], we propose a novel adaptive channel transform block (CTB). The CTB shares the macro architecture of STB, where non-linear embedding and gate block are also employed. Specifically, channel importance factors are generated based on the condition in a progressive down-sampling manner, and then multiplying the latent representation with the generated factor.

To validate the effectiveness of proposed transform coding, we integrate proposed transform coding technique with the entropy models STF [7], ELIC [11], LIC-TCM [14] and obtain learned image compression models LLIC-STF, LLIC-ELIC, LLIC-TCM for fair comparisons with existing state-of-art-transform coding methods. Extensive experiments demonstrate that our models significantly improvements upon corresponding baselines, especially on high-resolution images. Our LLIC models achieve state-of-the-art performance regarding rate-distortion performance and model complexity (Fig. 1, 9, Table I).

Our contributions are as follows:

- We introduce the Spatial Transform Block, utilizing  $11 \times 11$  and  $9 \times 9$  large receptive field transform to reduce spatial redundancy. To our knowledge, this is the *first* time to employ large kernels in learned image compression community.
- We propose generating depth-wise convolutional weights in a progressive down-sampling manner, using the input itself as a condition, which makes CNNs adaptive.
- We propose the Channel Transform Block, which employs importance factors for self-conditioned adaptive channel-

wise bit allocation in a progressive down-sampling manner, using the input itself as a condition.

- We propose the use of the Depth-wise Residual Bottleneck to enhance the non-linearity and the Gate block for efficient point-wise interaction.
- Extensive experiments demonstrate our proposed LLIC-STF, LLIC-ELIC, LLIC-TCM have significant improvements over corresponding baselines, achieve state-of-the-art performances and better trade-off between performance and complexity.

## II. RELATED WORKS

### A. Learned Image Compression

Toderici *et al.* [27], [28] propose the first learned image compression model based on recurrent neural networks, which encodes the residual between the reconstruction and ground-truth iteratively. Currently, most of the end-to-end learned image compression models [1]–[5], [11], [12], [19] are based on auto-encoders, where the input image is first transformed to the latent space for entropy coding, and the decoded latent is inverse transformed to RGB color space. To enhance the performance, Ballé *et al.* [3] introduce a hyper-prior for more accurate entropy coding. Context modeling [4] is also utilized to explore the correlations between current symbols and decoded symbols. Minnen *et al.* [4] employs pixel-cnn [29] for serial context prediction. He *et al.* [30] propose checkerboard context partition for parallel context modeling. Minnen *et al.* [5] propose to conduct serial context modeling along the channel dimension for faster decoding. In addition, global context modeling [12], [13], [31] are also introduced to explore the correlations among distant symbols. Multi-dimensional context modeling is recent developed. He *et al.* [11] combines the checkerboard partition and channel-wise context modeling. Jiang *et al.* [12], [13] propose the multi-reference entropy modeling to capture the local, global, and channel-wise correlations in an entropy model.

### B. Learned Transform Coding

The advantage of end-to-end learned image compression over non-learned codecs is its non-linear transform coding [17]. Transform plays an important role in improving the rate-distortion performance. For enhanced non-linearity, techniques such as generalized divisive normalization (GDN) [32] and Residual Bottleneck [33] have been utilized in learned image compression. Moreover, innovative normalization methods [34] have been proposed in recent years. Furthermore, Cheng *et al.* [19] suggest employing pixel shuffle for improved up-sampling. Some works [20], [35], [36] are proposed for better interactions between high-frequency and low-frequency features. For example, Akbari *et al.* [35] propose to employ octave convolution [37] to preserve more spatial structure of the information. Gao *et al.* [36] decompose the images into several layers with different frequency attributes for greater adaptability. Xie *et al.* [21] propose to adopt invertible neural networks to reduce information loss during transform. Inspired by non-learned codecs, wavelet-like transform [38] is also introduced in recent years. In addition to this, non-local attention [25],

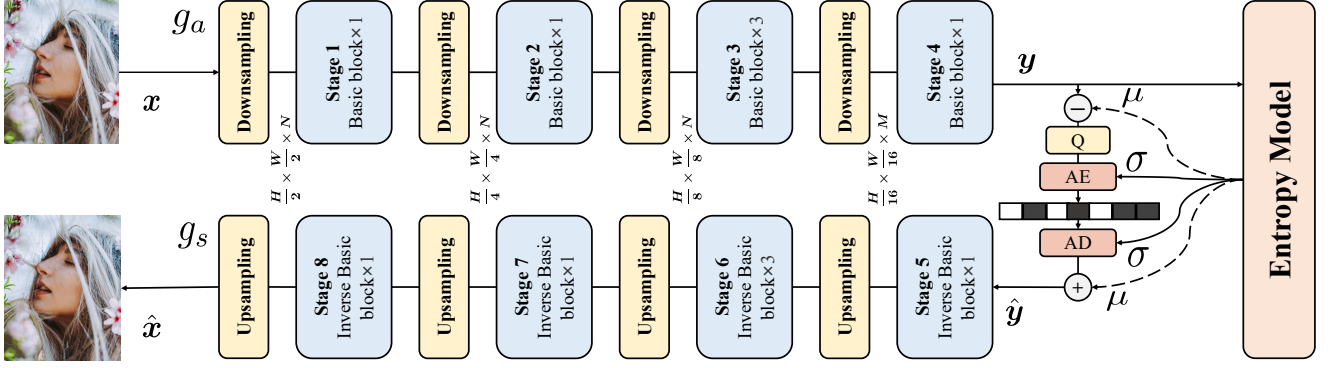


Fig. 2. Network architecture of our LLIC-STF, LLIC-ELIC, and LLIC-TCM.  $g_a$  is the analysis transform.  $g_s$  is the synthesis transform.  $Q$  is quantization.  $\mu$  and  $\sigma$  are the estimated mean and scale of latent  $\tilde{y}$  for probability estimation. Following baseline models, the latent representation  $y$  subtracts the means  $\mu$  for quantization before arithmetic encoding (AE) and the decoded residual  $Q(y - \mu)$  adds the means  $\mu$  after arithmetic decoding (AD).  $N = 192$ ,  $M = 320$ .

simplified attention [19], and group-separated attention [31] are employed to reduce more spatial redundancy. However, such attention mechanisms are much heavier and lead to higher complexity. Transformers [39], [40] have been employed in several works [6], [7], [14]. They stack swin-transformer [40] layers in transforms to reduce more redundancy. The dynamic weights and large receptive field of transformers contribute significantly to the overall performance enhancement.

However, to our knowledge, the large kernels are still not explored in learned image compression. Employing large kernels may lead to larger effective receptive fields, which implies that more redundancy can be reduced. Furthermore, how to utilize large kernels without leading to high complexity is *non-trivial*.

### III. METHOD

#### A. Problem Formulation

The formulation of end-to-end optimized image compression is first introduced. The basic process of end-to-end optimized learned image compression consists of an analysis transform  $g_a$ , a synthesis transform  $g_s$ , and an entropy model  $p$ . The entropy model  $p$  computes the means  $\mu$  and scales  $\sigma$  for probability estimation. The input image  $x$  is first transformed to latent representation  $y$  via analysis transform  $g_a$ . Latent representation is quantized to  $\hat{y}$  for entropy coding. The  $\hat{y}$  is inverse transformed to reconstructed image  $\hat{x}$  via the synthesis transform  $g_s$ . During training, the quantization is replaced by adding uniform noise (AUN) [3] or straight through estimator (STE) [2] for differentiability. In particular, adding uniform noise  $u \sim \prod \mathcal{U}(-0.5, 0.5)$  to latent representation makes the model related to VAEs [16]. The rate-distortion optimization in image compression is equivalent to evidence lower bound (ELBO) optimization in VAEs:

$$\begin{aligned} \mathcal{L} &= -(\mathcal{R} + \lambda \times \mathcal{D}) \\ &= \mathbb{E}_{q(\tilde{y}|x)} \left[ \underbrace{\log p(x|\tilde{y})}_{\text{distortion}} + \underbrace{\log p(\tilde{y})}_{\text{rate}} - \underbrace{\log q(\tilde{y}|x)}_0 \right]. \end{aligned} \quad (1)$$

The  $\log p(x|\tilde{y})$  is considered as distortion because

$$p(x|\tilde{y}) = \mathcal{N}(x|\tilde{x}, (2\lambda)^{-1}\mathbf{1}), \quad (2)$$

which is mean square error (MSE).  $\mathbb{E}_{q(\tilde{y}|x)} \log p(\tilde{y})$  is the cross entropy, which is the theoretical bound of entropy coding.

$$q(\tilde{y}|x) = q(\tilde{y}|y) = \mathcal{U}(\tilde{y}|y - 0.5, y + 0.5) = 1. \quad (3)$$

Current most of the learned image compression models [3]–[5], [7], [11], [12], [19], [21] also incorporate with hyper-priors [3]. The side information  $z$  is extracted from  $y$  using hyper-prior network. The side information  $\tilde{z}$  or  $\hat{z}$  helps estimate the entropy of latent  $\tilde{y}$  or  $\hat{y}$ . The loss function during training becomes

$$\begin{aligned} \mathcal{L} &= -(\mathcal{R} + \lambda \times \mathcal{D}) \\ &= \mathbb{E}_{q(\tilde{y}, \tilde{z}|x)} \left[ \underbrace{\log p(x|\tilde{y})}_{\text{distortion}} + \underbrace{\log p(\tilde{y}|\tilde{z}) + \log p(\tilde{z})}_{\text{rate}} \right. \\ &\quad \left. - \underbrace{\log q(\tilde{y}|x) + \log q(\tilde{z}|y)}_0 \right]. \end{aligned} \quad (4)$$

Compared with traditional image codecs [15], [41]–[43], the advantage of the learned image compression is its *non-linear* transform coding [17]. In such framework, the analysis transform and synthesis transform play an important role.

Firstly, the transform is employed to de-correlate the input image. The more the correlations are reduced, the more compact latent representation can be obtained, which reduces the bit-rate for compression. However, the receptive fields of most of the learned image compression models are still limited, which makes there are still certain redundancies in latent representation. In addition, most of the weights of transform modules are fixed during inference. The lack of context adaptability hinders the performance.

Secondly, from the perspective of generative models, the synthesis transform can be considered as a generator, which has significant influence on the reconstructed quality. A more powerful synthesis transform is able to generate more detailed details from input latent representation  $\hat{y}$ .

Thirdly, most of the analysis transforms down-sample the input for four times, which makes the resolution of the latent representation  $y$  is much smaller than that of the input image  $x$ . Most of the complexity of the image compression model is due to the transform coding. Taken Cheng'20 [19] as an example, the forward MACs of the Cheng'20 is 415.61 GMACs and

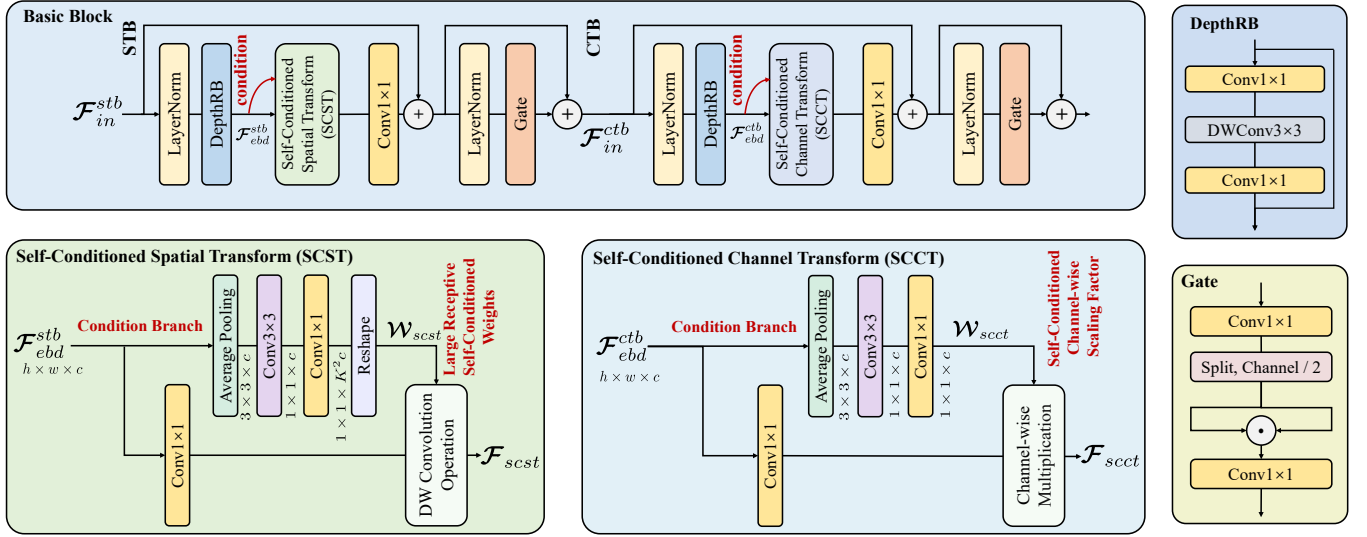


Fig. 3. Architecture of the proposed basic block. STB is the proposed Spatial Transform Block. CTB is the proposed Channel Transform Block. DepthRB is the depth-wise residual block for non-linear embedding. Gate is the proposed Gate Block.  $\mathcal{F}_{in}^{stb}$  is the input of STB.  $\mathcal{F}_{in}^{ctb}$  is the input of CTB.

the forward MACs of the entropy model is only 0.53 GMACs when the input is a  $768 \times 512$  image. Therefore, designing a more power transform module to reduce redundancies while maintaining modest model complexity is *non-trivial*. The challenges, along with the potential to further enhance the rate-distortion performance of learned image compression, motivate us to design the large receptive field transform coding with self-conditioned adaptability for learned image compression.

### B. Overview of Our Approach

The overall architecture of proposed LLIC-STF, LLIC-ELIC, LLIC-TCM is presented in Fig. 2 and Fig. 3. Our baseline models contain three kinds of state-of-the-art transform coding techniques. STF [7] employs transformers [40] for more compact latent representation. ELIC [11] employs residual convolutional layers and attention techniques [19] to enhance the non-linearity. LIC-TCM [14] employs the mixed CNN-transformer architectures to focus on the local and non-local redundancies. For fair comparisons with existing transform coding techniques, the entropy model of LLIC-STF, LLIC-ELIC, LLIC-TCM is aligned with the entropy model of STF [7], ELIC [11], and LIC-TCM [14], respectively.

Following our baseline models and existing methods [3]–[5], [12], [19], our proposed analysis transform and synthesis transform contain four stages. In each stage, the input is down-sampled or up-sampled by a downsampling block or an upsampling block. The down-sampling and up-sampling block contain a convolutional layer and a depth-wise residual bottleneck [11]. After down-sampling and up-sampling, the feature is fed into the basic blocks or inverse basic blocks. The basic block contains a Spatial Transform Block (STB) and a Channel Transform Block (CTB). The structures of inverse basic block and basic block are reversed, where the positions of STB and CTB are switched. The structures of STB and CTB follow the classic architecture of Transformers [39], [40]. STB and CTB employ layer normalization [44]. STB

and CTB contain a Depth-wise Residual Block (DepthRB) for embedding, main transform blocks and a gated block for point-wise interactions.

### C. Proposed Spatial Transform Block (STB)

The architecture of STB is in Figure 3. Depth Residual Block (DepthRB) is proposed for *non-linear* embedding. A Gate Block is proposed for efficient point-wise interactions with low complexity. We propose the Self-Conditioned Spatial Transform (SCST) to effectively reduce spatial redundancy. The overall process is formulated as:

$$\begin{aligned}\mathcal{F}_{ebd}^{stb} &= \text{DepthRB}(\text{Norm}(\mathcal{F}_{in}^{stb})), \\ \mathcal{F}_{scst} &= \text{SCST}(\mathcal{F}_{ebd}^{stb}), \\ \mathcal{F}_{mid}^{stb} &= \text{Conv1} \times 1(\mathcal{F}_{scst}) + \mathcal{F}_{in}^{stb}, \\ \mathcal{F}_{out}^{stb} &= \text{Gate}(\text{Norm}(\mathcal{F}_{mid}^{stb})) + \mathcal{F}_{mid}^{stb},\end{aligned}\quad (5)$$

where  $\mathcal{F}_{in}^{stb}$  is the input feature,  $\mathcal{F}_{out}^{stb}$  is the output feature.

1) *Nonlinear Embedding*: Previous works [7], [14], [39], [40] adopt one linear convolutional layer for embedding, in contrast to previous works, our STB uses a non-linear embedding method. We propose to employ the DepthRB. The architecture of DepthRB is presented in Figure 3, which contains a  $1 \times 1$  convolutional layer, a  $3 \times 3$  depth-wise convolutional layer, and a  $1 \times 1$  convolutional layer. The use of depth-wise convolution helps minimize complexity. The  $3 \times 3$  depth-wise convolutional layer helps aggregate more spatial information and the non-linearity enhances the expressiveness of the network.

2) *Self-Conditioned Spatial Transform (SCST)*: During transform, the more redundancies are reduced, the more compact latent representation we will obtain. However, existing state-of-the-art learned image compression models usually contain not large enough effective receptive fields, which are illustrated in Fig. 8. They [4], [5], [11], [19] usually employ  $3 \times 3$  or  $5 \times 5$  kernels. In addition, we find some transformer-based models



also suffer from not large enough receptive fields (Fig. 8). The limited receptive field makes there still exists redundancies. To achieve larger effective receptive field, we propose to employ depth-wise large kernels for analysis and synthesis transform. To our knowledge, this is the *first* attempt in learned image compression community to apply large kernels to transform. In our proposed transform coding method, the kernel size is enlarged to  $\{11, 11, 9, 9\}$  for different stages of analysis transform. The kernel sizes of the first two stages are larger because of the larger resolutions of input features of the first two stages. The large resolution features contains more spatial redundancies.

Although large kernels are employed in our proposed LLIC, the complexity is still modest due to the depth-wise connectivity. Assuming the large kernel size of a depth-wise convolution is  $K_L$  and the small kernel size of a vanilla convolution is  $K_S$ , and the input, output channel is  $N$ . The complexity of the large depth-wise convolution is  $K_L^2 \times N$  and the complexity of small vanilla convolution is  $K_S^2 \times N^2$ .

$$\begin{aligned} K_L^2 \times N &\geq K_S^2 \times N^2, \\ K_L &\geq K_S \sqrt{N}. \end{aligned} \quad (6)$$

The  $N$  is 192 in our LLIC models and our baselines [3]–[5], [7], [11], [19] and  $\sqrt{192} \approx 13.86$ , indicating that a  $11 \times 11$  depth-wise convolution is lighter than a  $1 \times 1$  vanilla convolution.

However, compared with existing transformer-based or attention-based transform coding techniques, the fixed kernel weights of convolutional layers cannot fully utilize the characteristics of the input image or feature. To this end, we propose to generate the convolutional weights through treating the input itself as the condition in a progressive down-sampling manner. The condition branch in SCST is utilized to generate the self-conditioned adaptive weights. Specifically, the input feature  $\mathcal{F}_{ebd}^{stb} \in \mathbb{R}^{c \times h \times w}$  is first average pooled to  $\mathcal{F}_{pool}^{stb} \in \mathbb{R}^{c \times 3 \times 3}$ , where  $c, h, w$  is the channel number, height, width of the  $\mathcal{F}_{ebd}^{stb}$ , respectively. The self-conditioned adaptive weights  $\mathcal{W}_{scst} \in \mathbb{R}^{c \times K^2}$  is computed via the convolution between the average pooled feature  $\mathcal{F}_{pool}^{stb}$  and the weights of condition branch, where  $K$  is the kernel size.

The overall process of proposed SCST is formulated as:

$$\begin{aligned} \mathcal{F}_{pool}^{stb} &= \text{AvgPool}(\mathcal{F}_{ebd}^{stb}), \\ \mathcal{W}_{scst} &= \text{Conv1} \times 1(\text{Conv3} \times 3(\mathcal{F}_{pool}^{stb})), \\ \mathcal{F}_{scst} &= \mathcal{W}_{scst} \otimes \text{Conv1} \times 1(\mathcal{F}_{ebd}^{stb}), \end{aligned} \quad (7)$$

where  $\mathcal{F}_{scst}$  is the output feature,  $\otimes$  is the convolution operation.

3) *Gate Mechanism*: In previous works [6], [7], feed forward network (FFN) [39] is adopted for channel-wise interactions, which contains two liner layer and a GELU [45] activation function. The overall process of a FFN is

$$\begin{aligned} \mathcal{F}_{inc}^{gate} &= \text{Conv1} \times 1(\mathcal{F}_{in}^{gate}), \\ \mathcal{F}_{act}^{gate} &= \frac{1}{2} \mathcal{F}_{inc}^{gate} \left( 1 + \tanh \left[ \sqrt{\frac{2}{\pi}} \left( 0.044715 (\mathcal{F}_{inc}^{gate})^3 \right) \right] \right), \\ \mathcal{F}_{out}^{gate} &= \text{Conv1} \times 1(\mathcal{F}_{act}^{gate}) + \mathcal{F}_{in}^{gate}, \end{aligned} \quad (8)$$

where  $\mathcal{F}_{in}^{gate} \in \mathbb{R}^{c \times h \times w}$  is the input feature,  $\mathcal{F}_{out}^{gate} \in \mathbb{R}^{c \times h \times w}$  is the output feature. Following existing methods, the channel number of  $\mathcal{F}_{inc}^{gate}$  and  $\mathcal{F}_{act}^{gate}$  is  $2c$ . The first  $1 \times 1$  convolutional layer increases the dimension of the input and the second  $1 \times 1$  convolutional layer decreases the dimension to the original dimension. The GELU [45] is much more complex than ReLU [46] or LeakyReLU. The GELU function can be simplified as  $\mathcal{F}_{inc}^{gate} \Phi(\mathcal{F}_{inc}^{gate})$  [47], which is quite similar to Gate mechanism. Replacing GELU with gate mechanism leads to lower complexity, which inspired us to employ a gate block instead of a FFN. The architecture of our Gate Block is illustrated in Figure 3. Specifically, the  $\mathcal{F}_{mid}^{gate}$  is split into two features  $\mathcal{F}_1^{gate} \in \mathbb{R}^{c \times h \times w}$  and  $\mathcal{F}_2^{gate} \in \mathbb{R}^{c \times h \times w}$  along the channel dimension. The activated feature  $\mathcal{F}_{act}^{gate}$  is obtained via the Hadamard product between  $\mathcal{F}_1^{gate}$  and  $\mathcal{F}_2^{gate}$ . The gate mechanism brings non-linearity, which is similar with GELU. The learnable  $1 \times 1$  convolutional layer also makes the proposed gate mechanism more flexible. The overall process of proposed Gate block is

$$\begin{aligned} \mathcal{F}_{inc}^{gate} &= \text{Conv1} \times 1(\mathcal{F}_{in}^{gate}), \\ \mathcal{F}_1^{gate}, \mathcal{F}_2^{gate} &= \text{Split}(\mathcal{F}_{inc}^{gate}), \\ \mathcal{F}_{act}^{gate} &= \mathcal{F}_1^{gate} \odot \mathcal{F}_2^{gate}, \\ \mathcal{F}_{out}^{gate} &= \text{Conv1} \times 1(\mathcal{F}_{act}^{gate}) + \mathcal{F}_{in}^{gate}. \end{aligned} \quad (9)$$

The complexity of a FFN is about  $O(4c^2hw + 2chw)$  while the complexity of proposed Gate block is  $O(3c^2hw + chw)$ . The Gate block is more efficient.

#### D. Proposed Channel Transform Block (CTB)

In proposed STB, the kernel weights are depth-wise connected, which means the interactions among channels should be improved. Compared to baseline models and existing learned image compression models, proposed STB employs much larger kernels, which means at the same depth, proposed STB can get a greater receptive field. The much greater receptive fields leave the room to enhance the channel interactions. Our proposed CTB is illustrated in Figure 3. The architecture of CTB is similar to STB. The SCST in STB is replaced with Self-Conditioned Channel Transform (SCCT) to build the CTB. The DepthBlock for non-linear embedding and Gate block are also employed. The overall process is formulated as

$$\begin{aligned} \mathcal{F}_{ebd}^{ctb} &= \text{DepthRB}(\text{Norm}(\mathcal{F}_{in}^{ctb})), \\ \mathcal{F}_{scst} &= \text{SCCT}(\mathcal{F}_{ebd}^{ctb}) \\ \mathcal{F}_{scst} &= \text{Conv1} \times 1(\mathcal{F}_{scst}) + \mathcal{F}_{in}^{ctb}, \\ \mathcal{F}_{out}^{ctb} &= \text{Gate}(\text{Norm}(\mathcal{F}_{scst})) + \mathcal{F}_{scst}, \end{aligned} \quad (10)$$

where  $\mathcal{F}_{in}^{ctb}$  is the input feature,  $\mathcal{F}_{out}^{ctb}$  is the output feature.

1) *Self-Conditioned Channel Transform (SCCT)*: In STB, large-receptive field kernels with self-conditioned adaptability are employed to reduce spatial redundancy. Due to the limited interactions among channels, Self-Conditioned Channel Transform (SCCT) is introduced to reduce channel-wise redundancy. For the feature  $\mathcal{F}_{ebd}^{ctb} \in \mathbb{R}^{c \times h \times w}$ , different channels have different information. The information of some channels is crucial for reconstruction while the information of some channels is

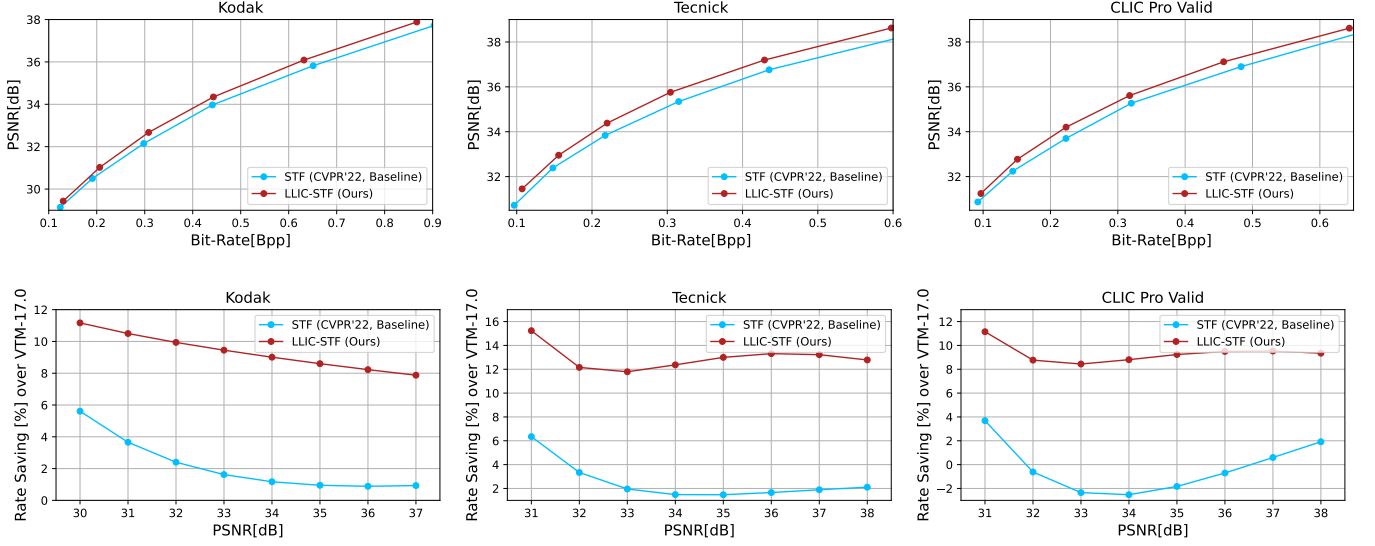


Fig. 4. PSNR-Bit-Rate curves and Rate saving-PSNR curves of our proposed LLIC-STF and its baseline STF [7]. The relative rate-saving curves are generated by first interpolating the discrete RD points with a cubic spline, and then compare bitrate of different models at fixed PSNR.

less useful. Allocating more bits to critical channels and fewer bits to non-critical channels saves bit-rate. To address this issue and inspired by Channel Attention [26], we propose to generate adaptive channel factors to modify the weights of channels. Proposed SCCT contains a condition branch and a main branch. In condition branch, the progressive down-sampling strategy is also adopted, which reduces information loss. The input feature  $\mathcal{F}_{ebd}^{ctb}$  is employed as condition. The  $\mathcal{F}_{ebd}^{ctb}$  is average pooled to reset the resolution and get  $\mathcal{F}_{pool}^{ctb} \in \mathbb{R}^{c \times 3 \times 3}$ . The self-conditioned channel scaling factor  $\mathcal{W}_{scct} \in \mathbb{R}^{c \times 1 \times 1}$  is computed via the convolution between  $\mathcal{F}_{pool}^{ctb}$  and weights of condition branch. The process is formulated as:

$$\begin{aligned} \mathcal{F}_{pool}^{ctb} &= \text{AvgPool}(\mathcal{F}_{ebd}^{ctb}), \\ \mathcal{W}_{scct} &= \text{Conv1} \times 1(\text{Conv3} \times 3(\mathcal{F}_{pool}^{ctb})), \\ \mathcal{F}_{scct} &= \mathcal{W}_{scct} \odot \text{Conv1} \times 1(\mathcal{F}_{ebd}^{ctb}), \end{aligned} \quad (11)$$

where  $\mathcal{F}_{scct}$  is the output feature. Since the channel factor is dependent of the condition, our proposed channel transform is adaptive.

#### E. Improved Training Techniques

In previous works, the kernel sizes are  $3 \times 3$  and  $5 \times 5$ , which is not enough for redundancy reduction. In our STB, the kernel size is scaled up to  $11 \times 11$  and  $9 \times 9$ , which further enlarge the receptive field. However, it is *non-trivial* to fully exploit the potential of large kernel. Vanilla training strategies (Using  $256 \times 256$  patches) adopted by previous works [7], [11], [19] cannot fully utilize the large convolutional kernel. When using  $256 \times 256$  patches, the resolutions of features during analysis transform are  $\{128 \times 128, 64 \times 64, 32 \times 32, 16 \times 16\}$ , which is too small, especially  $32 \times 32$  and  $16 \times 16$  for  $11 \times 11$  and  $9 \times 9$  kernels. To address this issue, we propose training using  $512 \times 512$  patches. To reduce computational overhead, we first train models on  $256 \times 256$  patches, then train models on  $512 \times 512$  patches. This approach is quite simple yet effective.

## IV. EXPERIMENTS

### A. Implementation Details

1) *Training dataset Preparation:* The proposed LLIC-STF, LLIC-ELIC, and LLIC-TCM are trained on 98939 images from COCO2017 [48], ImageNet [49], DIV2K [50], and Flickr2K [51]. The initial resolution of these training images are larger than  $512 \times 512$ . Following Ballé *et al* [3], in order to reduce compression artifacts that may be present in JPEG format images, JPEG images are further down-sampled with a randomized factor using PIL library. This down-sampling process ensures that the minimum height or width of the images falls within the range of 512 to 584 pixels.

2) *Training Strategy:* Our proposed LLIC-STF, LLIC-ELIC, and LLIC-TCM are built on Pytorch 2.1 [52] and CompressAI 1.2.0b3 [53]. Equation 4 is employed as the loss function. Following existing methods [3]–[5], [11], [12], [19], the MSE and Multi-Scale Structural Similarity (MS-SSIM) are employed as the distortion metrics during training for rate-distortion optimization. Following CompressAI [53], the  $\lambda$  in Equation 4 is set to  $\{18, 35, 67, 130, 250, 483\} \times 10^{-4}$  for MSE and  $\{2.4, 4.58, 8.73, 16.64, 31.73, 60.5\}$  for MS-SSIM. The training process is conducted on 2 Intel(R) Xeon(R) Platinum 8260 CPUs and 8 Tesla V100-32G GPUs under Pytorch distributed data parallel setting. During training, the batch-size is set to 16. Each model is trained for 2 M steps. The initial learning rate is  $10^{-4}$ . The learning rate drops to  $3 \times 10^{-5}$  at 1.7 M steps, drops to  $10^{-5}$  at 1.8 M steps, drops to  $3 \times 10^{-6}$  at 1.9 M steps, and finally drops to 1.95 M steps. Training images are randomly cropped to  $256 \times 256$  patches during the first 1.2M steps, and randomly cropped to  $512 \times 512$  patches during the rest steps. Large patches are employed to improve the performance of large receptive field transform coding.

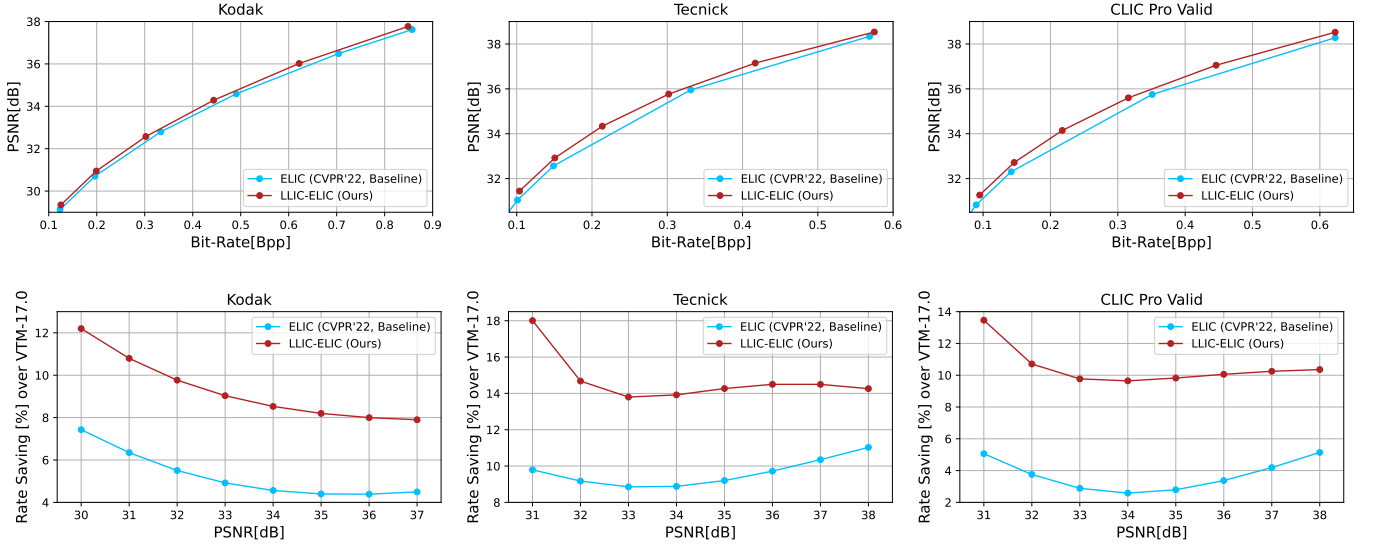


Fig. 5. PSNR-Bit-Rate curves and Rate saving-PSNR curves of our proposed LLIC-ELIC and its baseline ELIC [11].

## B. Test settings

1) *Performance Test Settings*: For models optimized for MSE, Peak Signal-to-Noise Ratio (PSNR) are utilized to measure distortion. The bits per pixel (Bpp) are utilized to measure bit-rate. The rate-distortion performances are measure on 5 widely used datasets, including

- Kodak [54] which contains 24 uncompressed images are widely used in learned image compression community [1], [3]–[7], [11], [12], [19], [21], [35], [38], [55]–[58]. The resolution of images in Kodak is  $768 \times 512$ .
- Tecnick [59] which contains 100 uncompressed images are utilized for performance evaluation in many previous works [4], [5], [14], [21], [60]. The resolution of images in Tecnick is  $1200 \times 1200$ .
- CLIC Pro Valid [18] and CLIC 2021 Test [61] are the validation dataset of 3th Challenge on Learned Image Compression and the test dataset of 4th Challenge on Learned Image Compression. CLIC Pro Valid contains 41 high-resolution images and CLIC 2021 Test contains 60 high-resolution images. Due to the impact of Challenge on Learned Image Compression, CLIC datasets are widely employed for rate-distortion evaluation [7], [8], [10], [11], [14], [19]. The average resolution of images in CLIC datasets is about  $2048 \times 1370$ .
- JPEG AI Test [62] is the test dataset of MMSP 2020 Learning-based Image Coding Challenge, which contains 16 images. The largest resolution of images in JPEGAI Test is  $3680 \times 2456$ .

These test datasets with different resolution (from  $768 \times 512$  to  $3680 \times 2456$ ) offer a comprehensive evaluation of learned image compression models.

Bjontegaard delta rate (BD-rate) [63] is utilized to rank the performance of learned image compression models.

2) *Complexity Test Settings*: To comprehensively evaluate the complexities of various learned image compression models, 16 images with resolution larger than  $3584 \times 3584$

from LIU4K test split [64] are selected as the complexity test images. These 16 images are further center cropped to  $\{512 \times 512, 768 \times 768, 1024 \times 1024, 1536 \times 1536, 2048 \times 2048, 2560 \times 2560, 3072 \times 3072, 3584 \times 3584\}$  patches in order to cover the various resolutions of images that can be encountered in reality. The model complexities are evaluated from four perspectives, including the peak GPU memory during encoding and decoding, model Forward inference MACs, encoding time, as well as decoding time. Encoding and decoding time include entropy coding and decoding time to better match practical applications and realistic scenarios.

## C. Rate-Distortion Performance

1) *Quantitive Results*: We compare our proposed LLIC-STF, LLIC-ELIC, LLIC-TCM with their baseline models STF [7], ELIC [11], LIC-TCM [14], recent learned image compression models [5], [6], [8]–[10], [19], [21], [22], [58], [60], [65], and non-learned image codec VTM-17.0 Intra [15]. The rate-distortion curves and rate-savings-distortion curves are illustrated in Fig. 4, Fig. 5, and Fig. 6. The BD-rate reductions are presented in Table I. VTM-17.0 under *encoder\_intra\_vtm.cfg* in YUV444 color space is employed as anchor.

Compared with baseline model STF [7], our proposed LLIC-STF performs much better on all bit-rates. Our proposed LLIC-STF brings average improvements of 0.33, 0.47, 0.40, 0.50, 0.62 dB in PSNR compared to STF on Kodak [54], Tecnick [59], CLIC Pro Valid [18], CLIC 2021 Test, and JPEGAI Test [62], respectively. Our LLIC-STF reduces 7.2%, 10.88%, 9.81%, 11.01%, 12.34% more bit-rates on these datasets when the anchor is STF.

Compared with baseline model ELIC [11], our proposed LLIC-ELIC performs much better on all-bit-rates. Our proposed LLIC-ELIC brings average improvements of 0.19, 0.25, 0.29, 0.21, 0.39 dB PSNR compared to ELIC on on Kodak [54], Tecnick [59], CLIC Pro Valid [18], CLIC 2021 Test, and JPEGAI Test [62], respectively. Our LLIC-ELIC

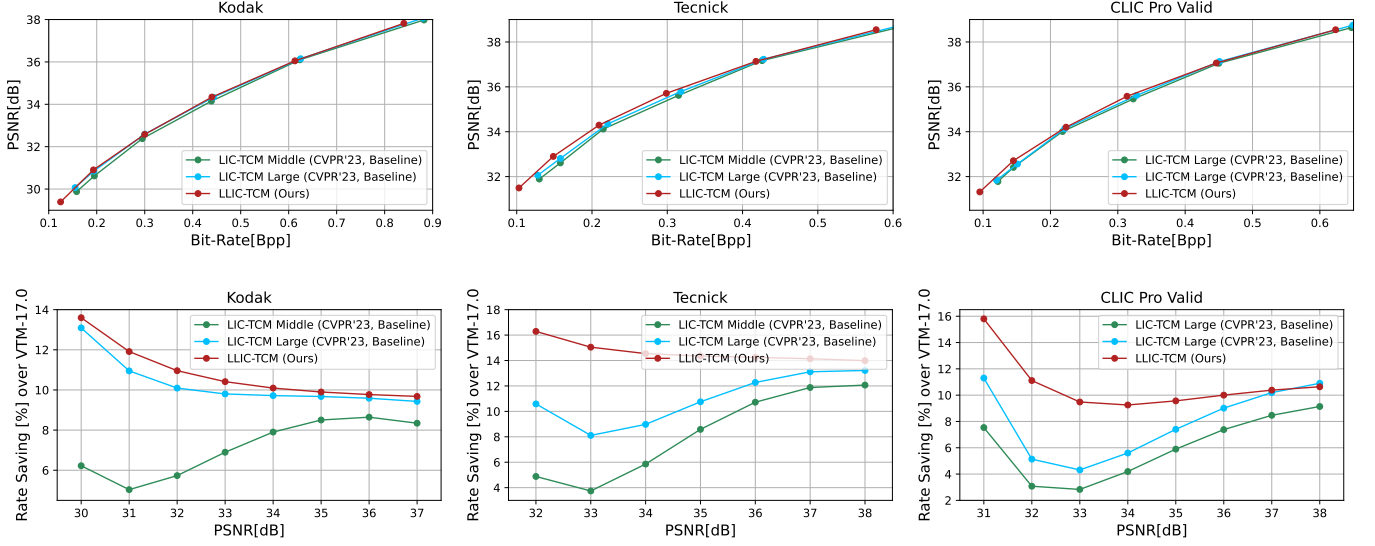


Fig. 6. PSNR-Bit-Rate curves and Rate saving-PSNR curves of our proposed LLIC-TCM and its baseline LIC-TCM [14]. We highlight the performance improvements over LIC-TCM Middle because the MACs of our LLIC-TCM is 321.93 G and the MACs of the LIC-TCM Middle is 415.2 G on Kodak. The MACs of LIC-TCM Large is 717.08 G on Kodak. Our LLIC-TCM also outperforms LIC-TCM Large with only half MACs of LIC-TCM Large.

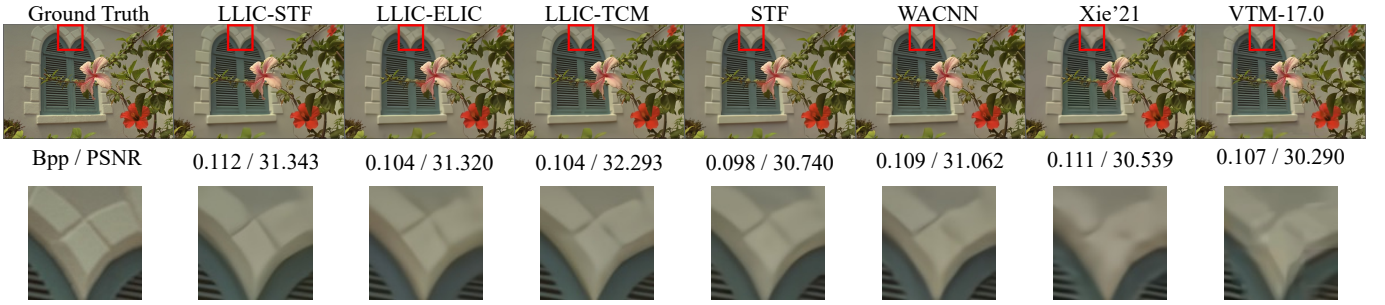


Fig. 7. Visualization of the reconstructed Kodim07 from the Kodak dataset. The metrics are [bpp↓/PSNR↑]. We compare our LLIC-STF, LLIC-ELIC, and LLIC-TCM with STF, WACNN [7], Xie'21 [21], and VTM-17.0 Intra [15].

reduces 4.25%, 5.66%, 7.11%, 4.80%, 8.54% more bit-rates on these datasets when the anchor is ELIC.

When comparing LLIC-TCM with LIC-TCM models, we highlight the performance improvements over LIC-TCM Middle because the MACs of our LLIC-TCM is 321.93 G and the MACs of the LIC-TCM Middle is 415.2 G. The MACs of LIC-TCM Large is 717.08 G. Our LLIC-TCM performs much better than LIC-TCM Middle and slightly better than LLIC-TCM Large on Kodak. Our proposed LLIC-TCM reduces more 3% bit-rates than LIC-TCM Middle and 1% than bit-rates than LIC-TCM Large. Our LLIC-TCM performs much better than LIC-TCM models on *high-resolution* images. Our LLIC-TCM reduces more 6%, 4% bit-rates than LIC-TCM Middle and 3.5%, 2.4% bit-rates than LIC-TCM Large on Tecnick and CLIC Pro Val, respectively. Our LLIC-TCM outperforms LIC-TCM Large with only half MACs of LIC-TCM Large.

2) *Qualitative Results*: Fig. 7 illustrates the example of reconstructed Kodim07 of our proposed models, WACNN, STF [7], Xie'21 [21], and VTM 17.0 Intra. PSNR value of the image reconstructed by our proposed models is 1 dB higher than image reconstructed by VTM 17.0 Intra. Compared with

STF, VTM 17.0 and other codecs, our proposed models can retain more details. Images reconstructed by our proposed LLIC have higher subjective quality.

#### D. Computational Complexity

The GPU Memory Consumption-Image Resolution, Forward MACs-Image Resolution, Encoding Time-Image Resolution, Decoding Time-Image Resolution curves are presented in Fig. 9. We compare our proposed LLIC-STF, LLIC-ELIC, LLIC-TCM with their baseline models STF [7], ELIC [11], LIC-TCM Large [14], and recent learned image compression models [19], [21], [22], [58], [65]. Overall, our proposed transform coding method enhance the model performance while exhibiting modest GPU memories, forward inference MACs, fast encoding and decoding speed.

1) *Testing GPU Memory Consumption Comparison*: Compared with existing recent learned image compression models Xie'21 [21], Entroformer [65], NeuralSyntax [66], Our proposed LLIC transform coding consumes much fewer GPU memories. When compressing  $3072 \times 3072$  images, the peak GPU memories of our proposed LLIC models are around



Methods	Kodak [54]		Tecnick [59]	CLIC Pro Valid [18]	CLIC 2021 Test [61]	JPEGAI Test [62]
	PSNR	MS-SSIM	PSNR	PSNR	PSNR	PSNR
VTM-17.0 Intra [15]	0.00	0.00	0.00	0.00	0.00	0.00
Cheng'20 (CVPR'20) [19]	+5.58	-44.21	+7.57	-39.61	+11.71	-41.29
Minnen'20 (ICIP'20) [5]	+3.23	-	-0.88	-	-	-
Qian'21 (ICLR'21) [58]	+10.05	-39.53	+7.52	-	+0.02	-
Xie'21 (ACMMM'21) [21]	+1.55	-43.39	+3.21	-	+0.99	-
Entroformer (ICLR'22) [65]	+4.73	-42.64	+2.31	-	-1.04	-
SwinT-Charm (ICLR'22) [6]	-1.73	-	-	-	-	-
NeuralSyntax (CVPR'22) [22]	+8.97	-39.56	-	-	+5.64	-38.92
McQuic (CVPR'22) [8]	-1.57	-47.94	-	-	+6.82	-40.17
Contextformer (ECCV'22) [9]	-5.77	-46.12	-9.05	-42.29	-	-
Pan'22 (ECCV'22) [60]	+7.56	-36.2	+3.97	-	-	-
NVTC (CVPR'23) [10]	-1.04	-	-	-	-3.61	-
<i>STF as Baseline</i>						
STF (CVPR'22) [7]	-2.48	-47.72	-2.75	+0.42	-0.16	+1.54
LLIC-STF (Ours)	<b>-9.49</b>	<b>-49.11</b>	<b>-13.06</b>	<b>-9.32</b>	<b>-11.44</b>	<b>-11.15</b>
<i>ELIC as Baseline</i>						
ELIC (CVPR'22) [11]	-5.95	-44.60	-9.14	-3.45	-7.52	-3.21
LLIC-ELIC (Ours)	<b>-9.47</b>	<b>-49.25</b>	<b>-14.68</b>	<b>-10.35</b>	<b>-12.32</b>	<b>-11.24</b>
<i>LIC-TCM as Baseline</i>						
LIC-TCM Middle (CVPR'23) [14]	-7.43	-	-8.99	-6.35	-	-
LIC-TCM Large (CVPR'23) [14]	-10.14	-48.94	-11.47	-8.04	-	-
LLIC-TCM (Ours)	<b>-10.94</b>	<b>-49.73</b>	<b>-14.99</b>	<b>-10.41</b>	<b>-13.14</b>	<b>-12.30</b>

TABLE I  
BD-RATE (%) COMPARISON FOR PSNR (dB) AND MS-SSIM. THE ANCHOR IS VTM-17.0 INTRA.

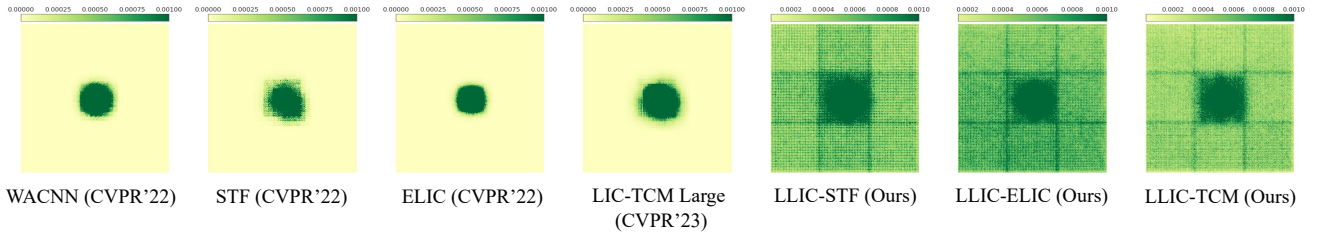


Fig. 8. Effective Receptive Fields of analysis transforms  $g_a$  of WACNN, STF, ELIC, LIC-TCM Large and our proposed models on 24 Kodak images center cropped to  $512 \times 512$ . The ERF is visualized as the absolute gradients of the center pixel in latent ( $d\mathbf{y}/d\mathbf{x}$ ) with respect to the input image.

10 GB, while the GPU memory consumption of Xie'21 [21] is over 20 GB. Compared to baseline models STF [7] and ELIC [11], our proposed LLIC-STF and LLIC-ELIC do not add much GPU memory overhead when compressing low resolution images. The GPU memory consumptions of STF, ELIC, LLIC-STF, and LLIC-ELIC are very close on low resolution images. It should be emphasized that our LLIC-STF and LLIC-ELIC have great performance improvements over STF [7] and ELIC [11], which illustrates the superiority of our approach. Compared to baseline model LIC-TCM Large [14], our LLIC-TCM significantly reduces the GPU memory consumption with better rate-distortion performance. When compressing and decompressing  $2048 \times 2048$  images, the GPU memory consumption of our proposed LLIC-TCM is

only  $\frac{1}{3}$  of the GPU memory consumption of LIC-TCM Large. When compressing  $3072 \times 3072$  images, the GPU memory consumption of our proposed LLIC-TCM is only  $\frac{1}{4}$  of the GPU memory consumption of LIC-TCM Large. The curve of the GPU memory consumed by our LLIC-TCM as the resolution grows is much flatter. The GPU memory overhead is a very important measure of model complexity because once the amount of GPU memory required for encoding or decoding exceeds the GPU memory capacity of the machine, it means that it is not possible to encode and decode images. The lower GPU memory consumption indicates that our proposed LLIC-STF, LLIC-ELIC, and LLIC-TCM have lower complexity and are highly suitable for high-resolution image compression.

2) *Forward Inference MACs Comparison:* The Forward Inference MACs of learned image compression models are

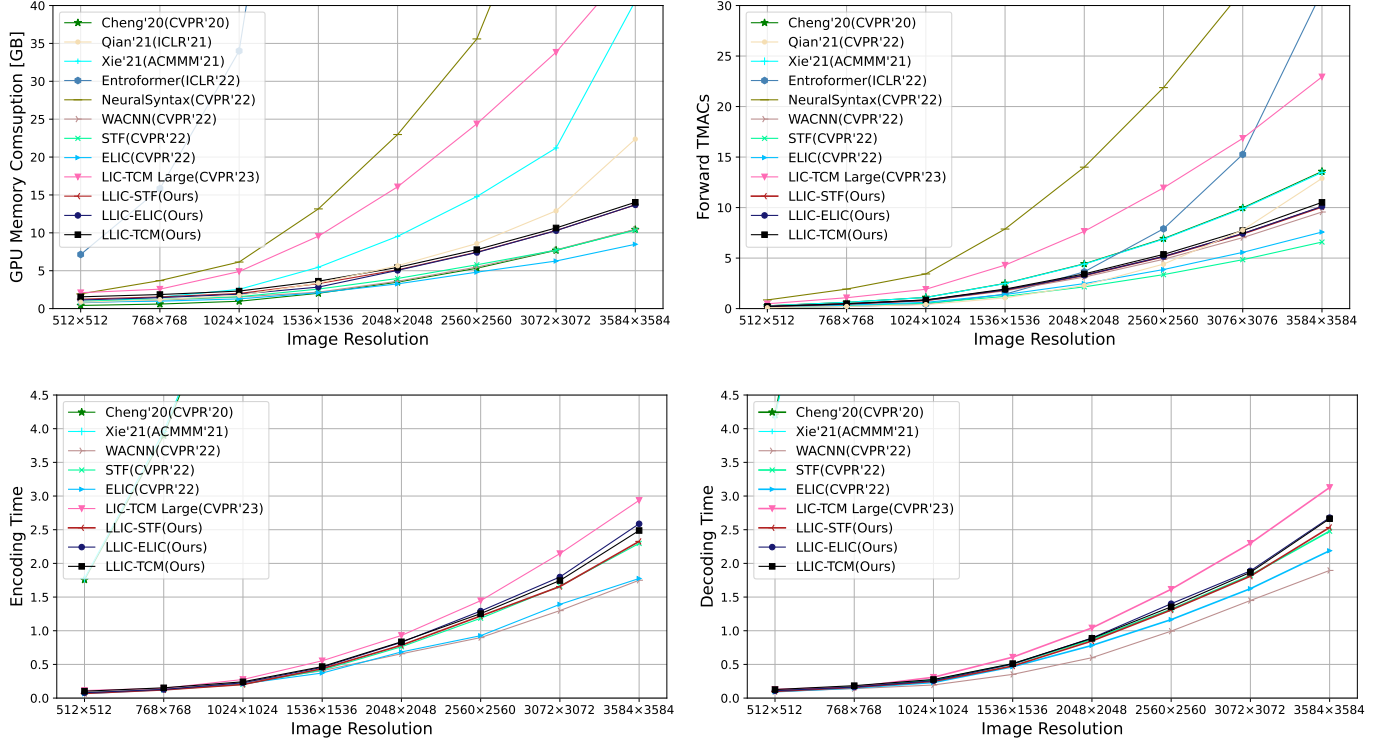


Fig. 9. GPU Memory Consumption-Image Resolution, Forward MACs-Image Resolution, Encoding Time-Image Resolution, Decoding Time-Image Resolution curves.

Settings	BD-Rate (%)	Forward MACs (G)
<b>LLIC-STF Basic Block</b>		
STB + STB	-6.05	331.55
CTB + CTB	-6.19	318.61
only CTB	-5.05	214.90
only STB	-4.19	221.29
<b>LLIC-STF w/o CTB</b>		
static weight	-2.58	221.26
w/o DepthRB	-1.01	188.09
w/o DepthRB & Gate	-0.18	198.83
<b>LLIC-STF w/o CTB</b>		
$K = \{5, 5, 5, 5\}$	+0.05	216.28
$K = \{7, 7, 7, 7\}$	-2.46	217.62
$K = \{9, 9, 9, 9\}$	-3.38	219.29
$K = \{11, 11, 9, 9\}$	-4.19	221.29
$K = \{11, 11, 11, 11\}$	-4.42	221.62
<b>LLIC-STF</b>		
$256 \times 256$ patch	-4.64	325.00
$512 \times 512$ patch	-7.85	325.00
VTM-17.0 Intra	0.00	—

TABLE II  
ABLATION STUDIES ON KODAK DATASET.

computed through the fvcare, DeepSpeed, Ptflops Library. Because the flops evaluation libraries are not very accurate, when evaluating one model, we compute the output values of fvcare, Deepspeed, Ptflops, and we take the average of the

two closest values as the final result. Compared with recent learned image compression models Cheng'20 [19], Xie'21 [21], Entroformer [65], and NeuralSyntax [22], our proposed LLIC-STF, LLIC-ELIC, LLIC-TCM exhibits much lower forward MACs. Specifically, the forward MACs of our proposed LLIC models are around  $\frac{1}{4}$  of the forward MACs of NeuralSyntax [22] when compressing  $2048 \times 2048$  images. Compared with baseline models STF [7], ELIC [11], our LLIC-STF, LLIC-ELIC have slightly higher forward MACs. Considering the performance gains of our proposed LLIC-STF, and LLIC-ELIC over STF [7], and ELIC [11], it is worthwhile to increase the forward MACs a bit, and besides, the forward MACs of our proposed LLIC models are around 74% of the forward MACs of Cheng'20 [19] when compressing  $2048 \times 2048$  images. Compared to baseline model LIC-TCM Large, our proposed LLIC-TCM significantly reduces the forward MACs. The forward MACs of our proposed LLIC-TCM is only 45% of the forward MACs of LIC-TCM Large when compressing  $2048 \times 2048$  images and compressing  $3072 \times 3072$  images. Compared with the mixed CNN-Transformer-based transform coding of LIC-TCM Large, our proposed large receptive field transform coding is more powerful and light-weight.

3) *Encoding and Decoding Time Comparison:* Since our LLIC-STF, LLIC-ELIC, LLIC-TCM employs parallel entropy models, our LLIC-STF, LLIC-ELIC, LLIC-TCM encode, decode much faster than Cheng'20 [19], Xie'21 [21], Qian'21 [58], Entroformer [65], and NeuralSyntax [22]. Specifically, when compressing a  $768 \times 768$  image, the encoding time of Cheng'20 and Xie'21 exceed 3s, the encoding time

of Qian'21 and Entroformer exceed 40s, the decoding time of Cheng'20 and Xie'21 exceed 7s and the decoding time of Qian'21 and Entroformer exceed 50s while the encoding and decoding time of our proposed LLIC models are around  $0.06 \sim 0.1$ s and  $0.1 \sim 0.12$ s. Compared to baseline model STF [7], our proposed LLIC-STF is about as fast as STF [7]. Compared to baseline model ELIC [11], our proposed LLIC-ELIC is about as fast as ELIC [11] on low resolution images. Our proposed LLIC-ELIC requires more 20% time and requires 7% to encode a  $2048 \times 2048$  image. The added time to encode and decode the high-resolution images is worthwhile considering the performance improvement brought about by our proposed transform coding. Compared with LIC-TCM Large, our LLIC-TCM encodes and decodes much faster than baseline model LIC-TCM Large. Overall, our proposed transform coding enhances the model performance while achieving fast encoding and decoding speed.

### E. Ablation Studies

1) *Settings*: The ablation studies are conducted on LLIC-STF. When conducting ablation experiments, we train each model for 1.7M steps from scratch. The batch size is set to 16. We adopt the training strategy in section IV-A2. The results of ablation studies is in Table II. In Table II, "w/o Gate" means the Gate block is replaced by a FFN [39].

2) *Influence of Self-Conditioned Spatial Transform*: Although it is possible to increase the theoretical receptive field by continuously stacking the network layers, it is likely that a small effective receptive field [23] will be obtained. Following Zhu *et al* [6], Effective Receptive Field (ERF) [23], [67] is employed to evaluate the influence of proposed self-conditioned spatial transform, which utilizes large depth-wise convolutions. The ERF is visualized as the absolute gradients of the center pixel in latent ( $dy/dx$ ) with respect to the input image. The ERFs of our baseline models STF [7], ELIC [11], LIC-TCM Large [14], our proposed LLIC-STF, LLIC-ELIC and LLIC-TCM are visualized in Fig. 8. Baseline model STF employs swin-transformer-based transform coding, ELIC employs CNN-Attention based transform coding, and the recent LIC-TCM employs mixed CNN-Transformer-based transform coding, and compared with these different kind of transform coding method, it is obvious that our proposed LLIC-STF, LLIC-ELIC, LLIC-TCM achieve much larger ERFs than their baselines. Larger ERFs indicate that our proposed large receptive field transform coding is able to remove more redundancy during the analysis transform, which makes our proposed models perform better than our baseline models.

To further investigate the contribution of proposed spatial transform block, spatial transform block is removed or replaced in our ablation studies. Specifically, removing STBs leads to significant performance degradation. If the STB is replaced by CTB, the rate-distortion performance is still not as good as the performance of the model utilizing STBs and CTBs. This performance degradation indicates the necessity of employing the proposed spatial transform blocks for a more compact latent representation to enhance the rate-distortion performance.

In our and baseline models, the analysis transform  $g_a$  and synthesis transform  $g_s$  contain four stages. The kernel

size of each stage is denoted as  $K = \{k_1, k_2, k_3, k_4\}$ . To evaluate the contribution of large kernel, we set to kernel size  $K = \{5, 5, 5, 5\}$ ,  $K = \{7, 7, 7, 7\}$ ,  $K = \{9, 9, 9, 9\}$ ,  $K = \{11, 11, 9, 9\}$ , and  $K = \{11, 11, 11, 11\}$ . The rate-distortion performances of utilizing various kernel sizes are shown in Table II. What is clear is that increasing the size of the convolutional kernel keeps improving the rate-distortion performance of the model, but the gains get smaller and smaller. Increasing kernel size  $K$  from  $\{5, 5, 5, 5\}$  to  $\{7, 7, 7, 7\}$  leads to the largest performance enhancement. The differences in the performance of utilizing  $\{11, 11, 9, 9\}$  kernels and the performance of utilizing  $\{11, 11, 11, 11\}$  kernels are quite negligible. Therefore, in our proposed LLIC models,  $K = \{11, 11, 9, 9\}$  is employed.

Context adaptability also plays an important role in boosting the rate-distortion performance of learned image compression models. When the kernel weights are independent on the input feature, the rate-distortion becomes worse. The rate-distortion performance loss is around 1.6%. The performance degradations demonstrate the effectiveness of the proposed self-conditioned weight generation.

3) *Influence of Self-Conditioned Channel Transform*: Channel transform block is proposed for self-conditioned adaptive channel adjustment. In ablation studies, channel transform blocks are removed or replaced. Specifically, removing CTBs leads to significant performance degradation and the rate-distortion performance of replacing CTBs with STBs is still not good as the performance of the model utilizing CTBs and STBs. The performance degradation in ablation studies demonstrates the effectiveness and necessity of employing channel transform block in transform coding.

4) *Influence of DepthRB and Gate Mechanism*: We conduct on LLIC-STF without CTBs to evaluate the effectiveness of proposed DepthRB for non-linear embedding. Compared with linear embedding, which employs a linear layer, our proposed DepthRB for non-linear embedding further enhance the rate-distortion performance. The non-linear embedding is more flexible than linear embedding. We also evaluate the effectiveness of proposed Gate block. Replacing the Gate blocks with vanilla FFNs makes the model more complex but leads to performance degradation, which demonstrate the superiority of the proposed Gate block.

5) *Influence of Large Patches for Training*: The  $256 \times 256$  patches are insufficient for training. To fully exploit large kernels, the large training strategy is employed. In our experiments, Using  $512 \times 512$  patches for training is enough and it brings a performance gain of close to 3%, which demonstrate the effectiveness of large patch training.

## V. CONCLUSION

In this paper, we propose large receptive-field transform coding with self-conditioned adaptability for learned image compression, which effectively capture more spatial correlations. To reduce channel-wise redundancy, we propose self-conditioned channel transform to adjust the weight of each channel. To evaluate our proposed transform method, we align the entropy model with existing advanced non-linear



transform coding techniques and obtain models LLIC-STF, LLIC-ELIC, LLIC-TCM. Extensive experiments demonstrate the superiority of our proposed large receptive field learning with self-conditioned adaptability. Our LLIC-STF, LLIC-ELIC, and LLIC-TCM achieve state-of-the-art performance and they reduce bd-rate by 9.49%, 9.47%, 10.94% on Kodak over VTM-17.0 Intra, respectively. To further enhance the performance, it is promising to integrate with more advanced entropy models [12], [13]. In addition, to make our model more practical, we will also investigate the asymmetrical architecture [68] between the encoder and the decoder.

## REFERENCES

- [1] J. Ballé, V. Laparra, and E. P. Simoncelli, “End-to-end optimized image compression,” in *International Conference on Learning Representations*, 2017.
- [2] L. Theis, W. Shi, A. Cunningham, and F. Huszár, “Lossy image compression with compressive autoencoders,” in *International Conference on Learning Representations*, 2017.
- [3] J. Ballé, D. Minnen, S. Singh, S. J. Hwang, and N. Johnston, “Variational image compression with a scale hyperprior,” in *International Conference on Learning Representations*, 2018.
- [4] D. Minnen, J. Ballé, and G. D. Toderici, “Joint autoregressive and hierarchical priors for learned image compression,” in *Advances in Neural Information Processing Systems*, 2018, pp. 10 771–10 780.
- [5] D. Minnen and S. Singh, “Channel-wise autoregressive entropy models for learned image compression,” in *2020 IEEE International Conference on Image Processing (ICIP)*. IEEE, 2020, pp. 3339–3343.
- [6] Y. Zhu, Y. Yang, and T. Cohen, “Transformer-based transform coding,” in *International Conference on Learning Representations*, 2022.
- [7] R. Zou, C. Song, and Z. Zhang, “The devil is in the details: Window-based attention for image compression,” in *In Proceedings of the IEEE conference on computer vision and pattern recognition*, 2022.
- [8] X. Zhu, J. Song, L. Gao, F. Zheng, and H. T. Shen, “Unified multivariate gaussian mixture for efficient neural image compression,” in *Proceedings of the IEEE/CVF Conference on Computer Vision and Pattern Recognition*, 2022, pp. 17 612–17 621.
- [9] A. B. Koyuncu, H. Gao, A. Boev, G. Gaikov, E. Alshina, and E. Steinbach, “Contextformer: A transformer with spatio-channel attention for context modeling in learned image compression,” in *European Conference on Computer Vision*, 2022, pp. 447–463.
- [10] R. Feng, Z. Guo, W. Li, and Z. Chen, “Nvtc: Nonlinear vector transform coding,” in *Proceedings of the IEEE/CVF Conference on Computer Vision and Pattern Recognition*, June 2023, pp. 6101–6110.
- [11] D. He, Z. Yang, W. Peng, R. Ma, H. Qin, and Y. Wang, “Elic: Efficient learned image compression with unevenly grouped space-channel contextual adaptive coding,” in *Proceedings of the IEEE/CVF Conference on Computer Vision and Pattern Recognition*, June 2022, pp. 5718–5727.
- [12] W. Jiang, J. Yang, Y. Zhai, P. Ning, F. Gao, and R. Wang, “Mlic: Multi-reference entropy model for learned image compression,” in *Proceedings of the 31st ACM International Conference on Multimedia*, 2023, pp. 7618–7627.
- [13] W. Jiang and R. Wang, “Mlic++: Linear complexity multi-reference entropy modeling for learned image compression,” *arXiv preprint arXiv:2307.15421*, 2023.
- [14] J. Liu, H. Sun, and J. Katto, “Learned image compression with mixed transformer-cnn architectures,” in *Proceedings of the IEEE/CVF Conference on Computer Vision and Pattern Recognition*, 2023, pp. 14 388–14 397.
- [15] B. Bross, Y.-K. Wang, Y. Ye, S. Liu, J. Chen, G. J. Sullivan, and J.-R. Ohm, “Overview of the versatile video coding (vvc) standard and its applications,” *IEEE Transactions on Circuits and Systems for Video Technology*, vol. 31, no. 10, pp. 3736–3764, 2021.
- [16] D. P. Kingma and M. Welling, “Auto-encoding variational bayes,” in *International Conference on Learning Representations*, 2014.
- [17] J. Ballé, P. A. Chou, D. Minnen, S. Singh, N. Johnston, E. Agustsson, S. J. Hwang, and G. Toderici, “Nonlinear transform coding,” *IEEE Journal of Selected Topics in Signal Processing*, vol. 15, no. 2, pp. 339–353, 2020.
- [18] G. Toderici, W. Shi, R. Timofte, L. Theis, J. Ballé, E. Agustsson, N. Johnston, and F. Mentzer, “Workshop and challenge on learned image compression (clic2020),” *CVPR*, 2020. [Online]. Available: [https://data.vision.ee.ethz.ch/cvl/clic/professional\\_valid\\_2020.zip](https://data.vision.ee.ethz.ch/cvl/clic/professional_valid_2020.zip)
- [19] Z. Cheng, H. Sun, M. Takeuchi, and J. Katto, “Learned image compression with discretized gaussian mixture likelihoods and attention modules,” in *Proceedings of the IEEE/CVF Conference on Computer Vision and Pattern Recognition*, June 2020.
- [20] F. Chen, Y. Xu, and L. Wang, “Two-stage octave residual network for end-to-end image compression,” in *Proceedings of the AAAI Conference on Artificial Intelligence*, vol. 36, 2022, pp. 3922–3929.
- [21] Y. Xie, K. L. Cheng, and Q. Chen, “Enhanced invertible encoding for learned image compression,” in *Proceedings of the ACM International Conference on Multimedia*, 2021, pp. 162–170.
- [22] D. Wang, W. Yang, Y. Hu, and J. Liu, “Neural data-dependent transform for learned image compression,” in *Proceedings of the IEEE/CVF Conference on Computer Vision and Pattern Recognition*, 2022, pp. 17 379–17 388.
- [23] W. Luo, Y. Li, R. Urtasun, and R. Zemel, “Understanding the effective receptive field in deep convolutional neural networks,” *Advances in neural information processing systems*, vol. 29, 2016.
- [24] Y. Zhang, K. Li, K. Li, B. Zhong, and Y. Fu, “Residual non-local attention networks for image restoration,” in *International Conference on Learning Representations*, 2018.
- [25] T. Chen, H. Liu, Z. Ma, Q. Shen, X. Cao, and Y. Wang, “End-to-end learnt image compression via non-local attention optimization and improved context modeling,” *IEEE Transactions on Image Processing*, vol. 30, pp. 3179–3191, 2021.
- [26] J. Hu, L. Shen, and G. Sun, “Squeeze-and-excitation networks,” in *Proceedings of the IEEE conference on computer vision and pattern recognition*, 2018, pp. 7132–7141.
- [27] G. Toderici, S. M. O’Malley, S. J. Hwang, D. Vincent, D. Minnen, S. Baluja, M. Covell, and R. Sukthankar, “Variable rate image compression with recurrent neural networks,” in *International Conference on Learning Representations*, 2016.
- [28] G. Toderici, D. Vincent, N. Johnston, S. Jin Hwang, D. Minnen, J. Shor, and M. Covell, “Full resolution image compression with recurrent neural networks,” in *Proceedings of the IEEE conference on Computer Vision and Pattern Recognition*, 2017, pp. 5306–5314.
- [29] A. Van den Oord, N. Kalchbrenner, L. Espeholt, O. Vinyals, A. Graves et al., “Conditional image generation with pixelcnn decoders,” *Advances in neural information processing systems*, vol. 29, 2016.
- [30] D. He, Y. Zheng, B. Sun, Y. Wang, and H. Qin, “Checkerboard context model for efficient learned image compression,” in *Proceedings of the IEEE/CVF Conference on Computer Vision and Pattern Recognition*, 2021, pp. 14 771–14 780.
- [31] Z. Guo, Z. Zhang, R. Feng, and Z. Chen, “Causal contextual prediction for learned image compression,” *IEEE Transactions on Circuits and Systems for Video Technology*, 2021.
- [32] J. Ballé, V. Laparra, and E. P. Simoncelli, “Density modeling of images using a generalized normalization transformation,” *arXiv preprint arXiv:1511.06281*, 2015.
- [33] K. He, X. Zhang, S. Ren, and J. Sun, “Deep residual learning for image recognition,” in *Proceedings of the IEEE conference on computer vision and pattern recognition*, 2016, pp. 770–778.
- [34] C. Shin, H. Lee, H. Son, S. Lee, D. Lee, and S. Lee, “Expanded adaptive scaling normalization for end to end image compression,” in *European Conference on Computer Vision*, 2022, pp. 390–405.
- [35] M. Akbari, J. Liang, J. Han, and C. Tu, “Learned multi-resolution variable-rate image compression with octave-based residual blocks,” *IEEE Transactions on Multimedia*, vol. 23, pp. 3013–3021, 2021.
- [36] G. Gao, P. You, R. Pan, S. Han, Y. Zhang, Y. Dai, and H. Lee, “Neural image compression via attentional multi-scale back projection and frequency decomposition,” in *Proceedings of the IEEE/CVF International Conference on Computer Vision*, 2021, pp. 14 677–14 686.
- [37] Y. Chen, H. Fan, B. Xu, Z. Yan, Y. Kalantidis, M. Rohrbach, S. Yan, and J. Feng, “Drop an octave: Reducing spatial redundancy in convolutional neural networks with octave convolution,” in *Proceedings of the IEEE/CVF international conference on computer vision*, 2019, pp. 3435–3444.
- [38] H. Ma, D. Liu, R. Xiong, and F. Wu, “iwave: Cnn-based wavelet-like transform for image compression,” *IEEE Transactions on Multimedia*, vol. 22, no. 7, pp. 1667–1679, 2019.
- [39] A. Vaswani, N. Shazeer, N. Parmar, J. Uszkoreit, L. Jones, A. N. Gomez, L. Kaiser, and I. Polosukhin, “Attention is all you need,” *Advances in neural information processing systems*, vol. 30, pp. 5998–6008, 2017.
- [40] Z. Liu, Y. Lin, Y. Cao, H. Hu, Y. Wei, Z. Zhang, S. Lin, and B. Guo, “Swin transformer: Hierarchical vision transformer using shifted windows,” in *Proceedings of the IEEE/CVF International Conference on Computer Vision (ICCV)*, October 2021, pp. 10 012–10 022.



- [41] W. B. Pennebaker and J. L. Mitchell, *JPEG: Still image data compression standard*. Springer Science & Business Media, 1992.
- [42] M. Rabbani, "Jpeg2000: Image compression fundamentals, standards and practice," *Journal of Electronic Imaging*, vol. 11, no. 2, p. 286, 2002.
- [43] G. J. Sullivan, J.-R. Ohm, W.-J. Han, and T. Wiegand, "Overview of the high efficiency video coding (hevc) standard," *IEEE Transactions on circuits and systems for video technology*, vol. 22, no. 12, pp. 1649–1668, 2012.
- [44] J. L. Ba, J. R. Kiros, and G. E. Hinton, "Layer normalization," *arXiv preprint arXiv:1607.06450*, 2016.
- [45] D. Hendrycks and K. Gimpel, "Gaussian error linear units (gelus)," *arXiv preprint arXiv:1606.08415*, 2016.
- [46] V. Nair and G. E. Hinton, "Rectified linear units improve restricted boltzmann machines," in *Proceedings of the 27th international conference on machine learning*, 2010, pp. 807–814.
- [47] L. Chen, X. Chu, X. Zhang, and J. Sun, "Simple baselines for image restoration," in *European Conference on Computer Vision*. Springer, 2022, pp. 17–33.
- [48] T.-Y. Lin, M. Maire, S. Belongie, J. Hays, P. Perona, D. Ramanan, P. Dollár, and C. L. Zitnick, "Microsoft coco: Common objects in context," in *European Conference on Computer Vision*, 2014, pp. 740–755.
- [49] J. Deng, W. Dong, R. Socher, L.-J. Li, K. Li, and L. Fei-Fei, "Imagenet: A large-scale hierarchical image database," in *2009 IEEE conference on computer vision and pattern recognition*. Ieee, 2009, pp. 248–255.
- [50] E. Agustsson and R. Timofte, "Ntire 2017 challenge on single image super-resolution: Dataset and study," *2017 IEEE Conference on Computer Vision and Pattern Recognition Workshops*, pp. 1122–1131, 2017.
- [51] B. Lim, S. Son, H. Kim, S. Nah, and K. Mu Lee, "Enhanced deep residual networks for single image super-resolution," in *Proceedings of the IEEE conference on computer vision and pattern recognition workshops*, 2017, pp. 136–144.
- [52] A. Paszke, S. Gross, F. Massa, A. Lerer, J. Bradbury, G. Chanan, T. Killeen, Z. Lin, N. Gimelshein, L. Antiga *et al.*, "Pytorch: An imperative style, high-performance deep learning library," in *Advances in Neural Information Processing Systems*, 2019, pp. 8024–8035.
- [53] J. Bégin, F. Racapé, S. Feltman, and A. Pushparaja, "Compressai: a pytorch library and evaluation platform for end-to-end compression research," *arXiv preprint arXiv:2011.03029*, 2020.
- [54] E. Kodak, "Kodak lossless true color image suite (photocd pcd0992)," 1993. [Online]. Available: <http://r0k.us/graphics/kodak/>
- [55] Z. Cheng, H. Sun, M. Takeuchi, and J. Katto, "Energy compaction-based image compression using convolutional autoencoder," *IEEE Transactions on Multimedia*, vol. 22, no. 4, pp. 860–873, 2020.
- [56] W. Yin, Y. Shi, W. Zuo, and X. Fan, "A co-prediction-based compression scheme for correlated images," *IEEE Transactions on Multimedia*, vol. 22, no. 8, pp. 1917–1928, 2020.
- [57] Y. Mei, L. Li, Z. Li, and F. Li, "Learning-based scalable image compression with latent-feature reuse and prediction," *IEEE Transactions on Multimedia*, vol. 24, pp. 4143–4157, 2022.
- [58] Y. Qian, Z. Tan, X. Sun, M. Lin, D. Li, Z. Sun, L. Hao, and R. Jin, "Learning accurate entropy model with global reference for image compression," in *International Conference on Learning Representations*, 2020.
- [59] N. Asuni and A. Giachetti, "Testimages: a large-scale archive for testing visual devices and basic image processing algorithms," in *STAG: Smart Tools & Apps for Graphics (2014)*, 2014.
- [60] G. Pan, G. Lu, Z. Hu, and D. Xu, "Content adaptive latents and decoder for neural image compression," in *European Conference on Computer Vision*, 2022, pp. 556–573.
- [61] G. Toderici, W. Shi, R. Timofte, L. Theis, J. Ballé, E. Agustsson, N. Johnston, and F. Mentzer, "Workshop and challenge on learned image compression (clic2021)," CVPR, 2021. [Online]. Available: [https://storage.googleapis.com/clic2021\\_public/professional\\_test\\_2021.zip](https://storage.googleapis.com/clic2021_public/professional_test_2021.zip)
- [62] JPEG-AI, "Jpeg-ai test images," [https://jpegai.github.io/test\\_images/](https://jpegai.github.io/test_images/), 2020.
- [63] G. Bjontegaard, "Calculation of average psnr differences between rd-curves," *VCEG-M33*, 2001.
- [64] J. Liu, D. Liu, W. Yang, S. Xia, X. Zhang, and Y. Dai, "A comprehensive benchmark for single image compression artifact reduction," *IEEE Transactions on image processing*, vol. 29, pp. 7845–7860, 2020.
- [65] Y. Qian, M. Lin, X. Sun, Z. Tan, and R. Jin, "Entroformer: A transformer-based entropy model for learned image compression," in *International Conference on Learning Representations*, 2022.
- [66] Z. Wang, E. P. Simoncelli, and A. C. Bovik, "Multiscale structural similarity for image quality assessment," in *The Thirty-Seventh Asilomar Conference on Signals, Systems & Computers*, 2003, vol. 2. Ieee, 2003, pp. 1398–1402.
- [67] X. Ding, X. Zhang, J. Han, and G. Ding, "Scaling up your kernels to 31x31: Revisiting large kernel design in cnns," in *Proceedings of the IEEE/CVF conference on computer vision and pattern recognition*, 2022, pp. 11 963–11 975.
- [68] Y. Yang and S. Mandt, "Computationally-efficient neural image compression with shallow decoders," in *Proceedings of the IEEE/CVF International Conference on Computer Vision (ICCV)*, 2023, pp. 530–540.